Soft Matter

PAPER

View Article Online
View Journal | View Issue

Cite this: *Soft Matter*, 2016, 12, 3352

Structural properties of polymer-brush-grafted gold nanoparticles at the oil–water interface: insights from coarse-grained simulations†

Xuebo Quan, ChunWang Peng, Jiaqi Dong and Jian Zhou*

In this work, the structural properties of amphiphilic polymer-brush-grafted gold nanoparticles (AuNPs) at the oil–water interface were investigated by coarse-grained simulations. The effects of grafting architecture (diblock, mixed and Janus brush-grafted AuNPs) and hydrophilicity of polymer brushes are discussed. Simulation results indicate that functionalized AuNPs present abundant morphologies including typical core–shell, Janus-type, jellyfish-like, *etc.*, in a water or oil–water solvent environment. It is found that hydrophobic/weak hydrophilic polymer-brush-grafted AuNPs have better phase transfer performance, especially for AuNPs modified with hydrophobic chains as outer blocks and weak hydrophilic chains as inner blocks. This kind of AuNP can cross the interface region and move into the oil phase completely. For hydrophobic/strong hydrophilic polymer-brush-grafted AuNPs, they are trapped in the interface region instead of moving into any phase. The mechanism of phase transfer is ascribed to the flexibility and mobility of outer blocks. Besides, we study the desorption energy by PMF analysis. The results demonstrate that Janus brush-grafted AuNPs show the highest interfacial stability and activity, which can be further strengthened by increasing the hydrophilicity of grafted polymer brushes. This work will promote the industrial applications of polymer-brush-grafted NPs such as phase transfer catalysis and Pickering emulsion catalysis.

Received 4th November 2015,
Accepted 25th February 2016

DOI: 10.1039/c5sm02721g

www.rsc.org/softmatter

1. Introduction

Polymer-brush-functionalized inorganic nanoparticles (NPs), also called hairy NPs, are composed of a core and a layer of polymer chains densely grafted by one end on the surface of core particles *via* a covalent bond, which have received much attention in nanomaterials science.[1–7] Featuring the stability of inorganic NPs and the versatility of polymer brushes, their properties can be tuned by altering the chemical nature, grafting density, chain length and grafting architecture of polymer brushes, or by changing the nanoparticle size, shape, *etc.*[8–10]

Recently, much attention has been focused on the interfacial behaviours of polymer-brush-grafted NPs at the liquid–liquid interface, which are of great significance in a broad range of applications such as phase transfer catalysis, Pickering emulsion, drug delivery and so on.[11–14] It is believed that the structure and interfacial activity of functionalized NPs can be influenced by the grafting architecture and hydrophilicity of polymer brushes.[15,16] As extensively demonstrated by Binks and co-workers,[15] NPs with different inherent wettabilities have been widely used to stabilize different types of emulsions, and the wettability can be tuned by grafting appropriate hydrophilic/hydrophobic polymer brushes on the NP surface. Miguel *et al.*[16] made a comparison of the interfacial activity between homogeneous gold nanoparticles and amphiphilic Janus gold nanoparticles by pendant drop tensiometry for the decane–water interface. They concluded that the latter exhibited a higher interfacial activity, demonstrating the importance of grafting architecture of polymer brushes. In most cases, NPs at the liquid–liquid interface are always trapped in the interface region as the surface energy of the nanoparticles cannot be easily changed to be suitable for each phase.[17] However, it has been reported that the phase transfer of NPs can be achieved by regulating the solvent composition, pH, temperature, *etc.*[13,18–24] For example, Niikura and co-workers[22] modified the surface of AuNPs with alkyl chain-*b*-PEG-*b*-alkyl chain triblock polymer brushes, and found that the amphiphilic hairy gold NPs can transfer from the water phase to the chloroform phase driven by the conformational change of the grafted chains. Duan *et al.*[23] synthesized binary mixed PEG/PDEAEMA homopolymer brush-functionalized AuNPs. The NPs remained in the aqueous phase under low pH conditions, while transferred from the water phase to the oil phase under high

School of Chemistry and Chemical Engineering, Guangdong Provincial Key Lab for Green Chemical Product Technology, South China University of Technology, Guangzhou, 510640, P. R. China. E-mail: jianzhou@scut.edu.cn

† Electronic supplementary information (ESI) available: Details of the nanoparticle setup, simulation methods and some analysis of the corresponding all-atom molecular simulation. See DOI: 10.1039/c5sm02721g

pH conditions. Li *et al.*[24] studied and confirmed that PNIPAM (poly(*N*-isopropylacrylamide)) polymer brush-grafted gold NPs can pass through the oil–water interface and transfer into the oil phase when the temperature was increased to above LCST.

Nevertheless, the structure and interfacial behaviours of polymer brush-grafted NPs at the liquid–liquid interface are difficult to be obtained from experiments at the molecular level. Computer simulations are ideally suited to complement this. Some theoretical models[25–29] have been conducted to explore the interaction of NPs with the liquid–liquid interface. Fan *et al.*[25] investigated the properties of 3 nm-diameter silica nanoparticles with different surface chemistry at the decane–water interface by using all-atom molecular dynamics (AAMD) simulations. AAMD may present more detailed molecular information; however, it is limited to systems containing tens to hundreds of thousands of atoms at the nano-second time-scale. Therefore, coarse-grained (CG) simulations are more appropriate for this complex system. Dissipative particle dynamics (DPD), first introduced by Hoogerbrugge and Koelman and then revised by Espanol and Warren,[30–32] is one of the most common CG methods, which has been widely employed in the self-assembly of polymers, drug delivery, polymer brush, *etc.*[33–36] Nie and co-workers[37,38] studied the self-assembly of amphiphilic AuNPs in selective solvents by combining experiments and DPD simulations. They demonstrated that NPs could form various morphologies including unimolecular micelles, clusters and vesicles, depending on the length of the polymer tethers and the size of the gold cores. The MARTINI CG force field was developed by Marrink and co-workers[39,40] who specialized in lipid membrane simulations and has been extended to include proteins,[41–43] polymers,[44,45] inorganic particles[46] and other systems.[47] Chan *et al.*[46] simulated the membrane and capsule formation of alkyl sulfhydryl modified AuNPs. Lin *et al.*[48,49] investigated the self-assembly behaviours of monolayer-protected AuNPs in solvent with different polarities and the interactions between short alkyl sulfhydryl modified AuNPs with the cell membrane. Dong and Zhou[50] performed CG simulations based on the MARTINI force field for PS/PEO polymer-brush-modified amphiphilic AuNPs to study their solvent-responsive behaviours, and typical core–shell, Janus-type, buckle-like, ring-like, jellyfish-like and octopus-like morphologies were formed depending on the solvent polarity and grafting architecture of polymer brushes. Then, they systematically studied the phase transfer behaviour of AuNPs modified with amphiphilic triblock brushes composed of different block components and block sequences at the oil–water interface.[51] They concluded that the AuNPs grafted with hydrophobic–weak hydrophilic–hydrophobic triblock copolymer brushes exhibit the best phase transfer performance; however, for NPs modified with weak hydrophilic–hydrophobic–weak hydrophilic triblock copolymer brushes, the phase transfer can hardly occur unless the extent of the hydrophobic block exceeds 60%. In addition, self-consistent field theory (SCFT) and Brownian dynamics (BD) have also been adopted.[52,53] Jason and co-workers[52] employed the SCFT method to describe the structure and the properties of fluid interfaces stabilized by nanoparticles functionalized with polymers of various grafting architectures, and demonstrated the important role played by the conformation of the grafted chains in the interfacial tension. Almusallam *et al.*[53] investigated the effects of the block sequence and interaction strength on interfacial behaviours of copolymer brush protected metal NPs at the oil–water interface.

To the best of our knowledge, rare research has been focused on the effect of grafting architecture and hydrophilicity of polymer brushes on the structure and interfacial behaviours of functionalized NPs at the oil–water interface. With the development of the grafted nanoparticle synthesis strategy, it has led to the possibility of complex grafting architectures such as NPs grafted with multiblock polymers, mixtures of several chemically distinct homopolymers, or "Janus" grafting.[52,54,55] In this work, we chose an AuNP as a model particle, which has been widely studied in many scientific and technological fields due to its excellent properties, and modified AuNPs by polymer brushes with different grafting architectures and hydrophilicity to form diblock brushes, mixed brushes and Janus-grafted AuNPs, and then investigate the structure and interfacial properties of these functionalized AuNPs at the oil–water interface by CG simulations.

2. Methods

2.1 Force fields

The MARTINI CG force field developed by Marrink *et al.*[39,40] was adopted to investigate the interfacial behaviours of polymer-brush-functionalized AuNPs with different grafting architectures at the oil–water interface. In the framework of this CG model, small groups of atoms are united as a single interaction site. In general, this model maps four heavy atoms into one CG particle, except for the case of ring structures (such as benzene and cholesterol), where a 2 or 3 to 1 mapping is adopted. Based on the differences of the chemical nature of the underlying structure, four main types of interaction sites are considered. The four types are polar (P), non-polar (N), apolar (C), and charged (Q), each of which has a number of sublevels to distinguish the hydrogen-bonding capabilities (d = donor, a = acceptor, da = both, and 0 = none) or the degree of polarity (1 to 5, from low polarity to high polarity). It is worth noting that because of the smoothed energy barrier in the MARTINI force field, the effective time that system has gone through is four times longer than the simulation sampling time,[39] thus we used effective time in this work.

2.2 Functionalized AuNP systems

A cuboctahedral AuNP structure which consists of 147 Au beads with a diameter of about 2.5 nm was adopted, the bond length between neighboring Au beads was set to 0.408 nm, the same as the lattice constant of the gold atom, and the force constant of the harmonic bonding potential is very high to keep the particle internally rigid, thus the gold core behaves as a solid particle, which is the same as that used in our previous studies.[50,51] It should be noted that the gold nanoparticle is only used as a

substrate to graft polymer brushes with high grafting density and long length, so the gold core has little impact on the structural properties of functionalized AuNPs. The SC4 particle type in the MARTINI force field was assigned for Au beads. For polymer brushes, a train-like single-bead chain model was used, and the hydrophobic chains were all made up of C1 beads (similar to alkyl chains), N0 beads (similar to PEO) and P2 beads (similar to PVA), to describe the weak and quite strong hydrophilic blocks. Each chain consists of 30 beads, and totally 32 polymer brushes were grafted on the surface of AuNPs as even as possible, thus the grafting density was about 1.63 chains per nm^2, which is reasonable according to the experimental data.[4] Four grafting schemes of polymer brushes were considered, namely two diblock brushes with different monomer sequences (AB brush: hydrophobic chains as inner blocks while weak hydrophilic chains as outer blocks; BA brush: hydrophobic chains as outer blocks while weak hydrophilic chains as inner blocks), evenly mixed architecture (hydrophilic and hydrophobic brushes evenly distributed on the gold surface, mixed brush) and Janus architecture (half hydrophilic brushes spaced on one side of the gold surface while half hydrophobic brushes located on another side, Janus brush). These four architectures are shown in Fig. 1. Water and oil solvents were represented by polar P4 beads and apolar C3 beads, respectively.[51]

2.3 Simulation details

In this work, we studied the structure and interfacial activity of diblock-, mixed- and Janus-brush-grafted AuNPs at the oil–water interface. For each functionalized AuNP, we created a cuboid simulation box with the dimensions of $18 \times 18 \times 36$ nm^3, and the functionalized AuNPs were put in the middle of the box with approximately 95 000 water beads. Then, 40 ns NPT-MD equilibration was performed with a time step of 20 fs to make sure that functionalized AuNPs were in equilibrium with the water environment. The systems were coupled with a Berendsen thermostat and barostat at 300 K and 1.0 bar. A cut-off distance of 1.2 nm was used for van der Waals (vdW) interactions. After equilibration in water, the NPs were placed at the oil–water interface and another 400 ns MD simulation was performed with the same parameters. The umbrella sampling technique and the weighted histogram analysis method were used to calculate the potential of mean force (PMF) for the transfer of functionalized AuNPs from the water phase to the oil phase, and the force constant of the harmonic potential was 1000 kJ mol^{-1} nm^{-2}. The starting configurations with a 0.2 nm step size were generated by an external force for acceleration. Each simulation was run for 400 ns. All CG simulation studies were performed by using the GROMACS 4.5.4 package.[56] For structure visualization, the Visual Molecular Dynamics (VMD) program was used.[57]

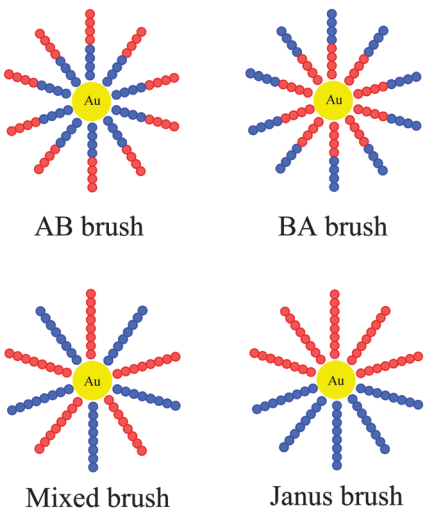

Fig. 1 Schematic representation of the polymer brush-grafted AuNP systems studied in this work. [A stands for hydrophobic beads (C1 beads, blue colour), while B denotes hydrophilic beads (N0 and P2 beads, red colour). Au beads are coloured in yellow].

3. Results and discussion

It has been demonstrated that CG models and methods are valid for describing the interaction of polymer-brush-grafted AuNPs at the oil–water interface.[51] Besides, we also performed all-atom MD simulations of a simple system for comparison, and a detailed description about the setup of the model and methods is given in the ESI.†

In this section, firstly, we analyzed the polymer brush distributions along the z axis by density profiles and described the morphologies of the functionalized AuNPs, which are important for the explanation of the mechanism of phase transfer behaviour and different structural properties of the studied systems. Equilibrium positions of functionalized AuNPs and the detailed phase transfer behaviour were also investigated. Besides, we computed the desorption energy required to move one functionalized AuNP from the interface region into the oil phase through PMF analysis, in order to make a comparison of the interfacial activity of functionalized AuNPs with different grafting architectures and hydrophilicity. The results are summarized in Fig. 2–5 and Tables 1 and 2.

3.1 Equilibrated morphologies of functionalized AuNPs

Hydrophobic/weak hydrophilic polymer brush-grafted AuNPs (C1/N0 systems). These model systems correspond to the AuNPs modified with hydrophobic chains and weak hydrophilic chains, which correspond to alkyl chain/PEG polymer brushes, as used by Niikura and co-workers.[22] As seen from Fig. 2, the functionalized AuNPs with different grafting architectures exhibit different morphologies both in the water phase and the oil–water biphase, and the relative positions of functionalized AuNPs at the oil–water interface are also quite unlike.

In a pure water environment, the functionalized AuNPs achieve equilibrium and all polymer brushes are bent on the surface of the gold core. For BA diblock polymer-brush-grafted AuNPs, hydrophobic blocks act as head ends and hydrophilic blocks act as tail ends, and a typical "Janus" conformation is formed, which is caused by the exposure of inner hydrophilic N0 blocks in water to reach thermodynamic stability. However, for

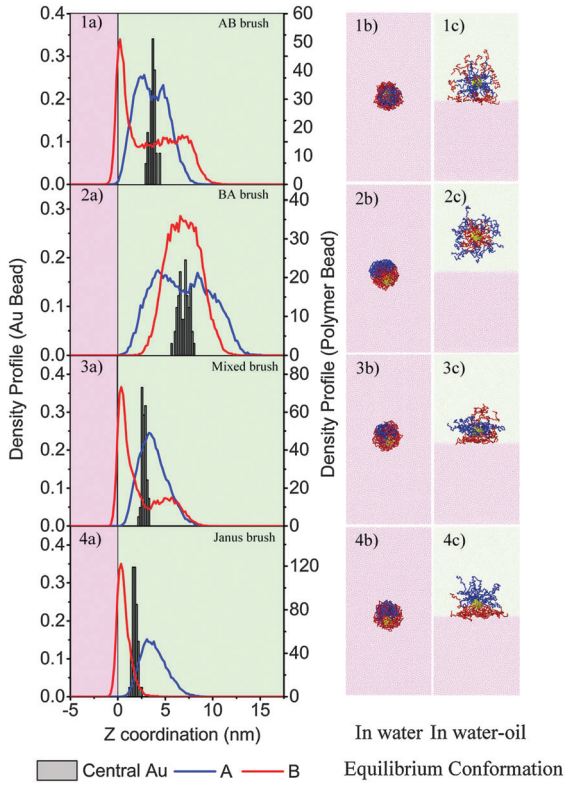

Fig. 2 Brush density profiles and equilibrium morphologies of functionalized NPs. [(a) Density profiles; (b) equilibrium morphologies in water system; (c) equilibrium morphologies in the oil–water two phase system. Water phase: pink colour, oil phase: green colour, hydrophobic chains: blue colour and weak hydrophilic chains: red colour].

Table 1 Equilibrium positions of AuNP centres of functionalized AuNPs studied in this work

	Systems	Equilibrium position (Z coordinate, nm)
C1/N0	AB brush	2.4
	BA brush	7.1
	Mixed brush	2.5
	Janus brush	1.8
C1/P2	AB brush	2.2
	BA brush	−0.5
	Mixed brush	0.6
	Janus brush	0.6

functionalized AuNPs in other three systems, classic core–shell structures with a hydrophobic C1 core and a hydrophilic N0 shell are developed. This unique morphology has been widely used in drug delivery vehicles. After being equilibrated in oil and water phases, functionalized AuNPs with various grafting architectures show considerable differences in the particle position and conformation. For AB and BA diblock polymer brush-grafted AuNPs, the former shapes into a core–shell structure with hydrophobic C1 blocks as cores and hydrophilic N0 blocks as shells, while the situation is just the opposite for the latter. Different morphologies are also formed for the mixed brush and Janus brush-modified NPs. A three-layer "hamburger" structure forms for the mixed brush-modified NPs while the

Table 2 Desorption energy of functionalized NPs estimated from PMF profiles

	Systems	Desorption energy (kcal mol^{-1})
C1/N0	AB brush	11.4
	BA brush	NA[a]
	Mixed brush	9.6
	Janus brush	22.4
C1/P2	AB brush	212.4
	BA brush	190.6
	Mixed brush	227.9
	Janus brush	244.9

[a] In this case, the functionalized AuNP can cross the interface region spontaneously without an applied pulling force, so the value is not given.

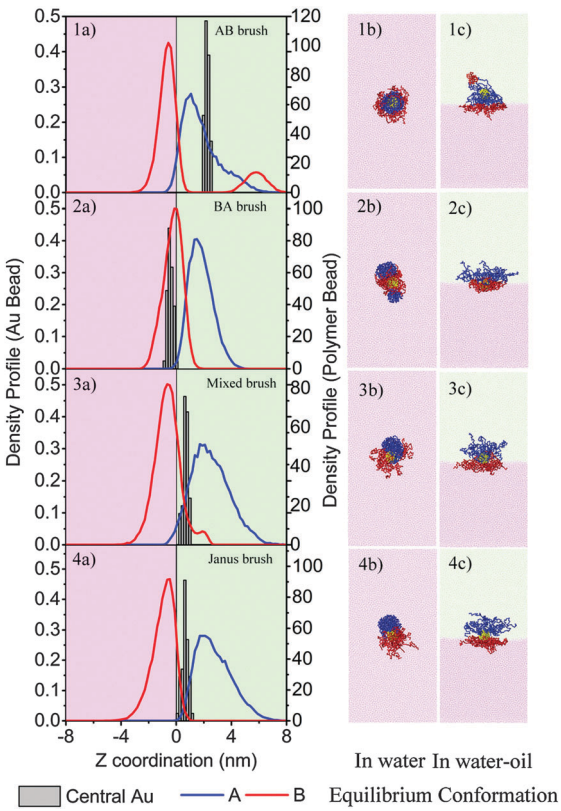

Fig. 3 Brush density profiles and equilibrium morphologies of functionalized NPs. [(a) Density profiles; (b) equilibrium morphologies in the water system; (c) equilibrium morphologies in the oil–water two phase system. Water phase: pink colour, oil phase: green colour, hydrophobic chains: blue colour and strong hydrophilic chains: red colour].

equilibrium conformation of the Janus brush-grafted AuNPs remains "Janus" morphology. In all cases, all brushes, which collapse on the solid surface in a water environment, are stretched out. In addition, it is interesting to find that the BA brush-grafted AuNPs can break into the interface region and transfer into the oil phase completely, while AuNPs in other three systems stand on the oil side because of the strong hydrophobicity of C1 chains; they cannot leave the interface region due to the hydrophilic chains being trapped in the water phase. The phase transfer behaviour of BA brush-grafted AuNPs

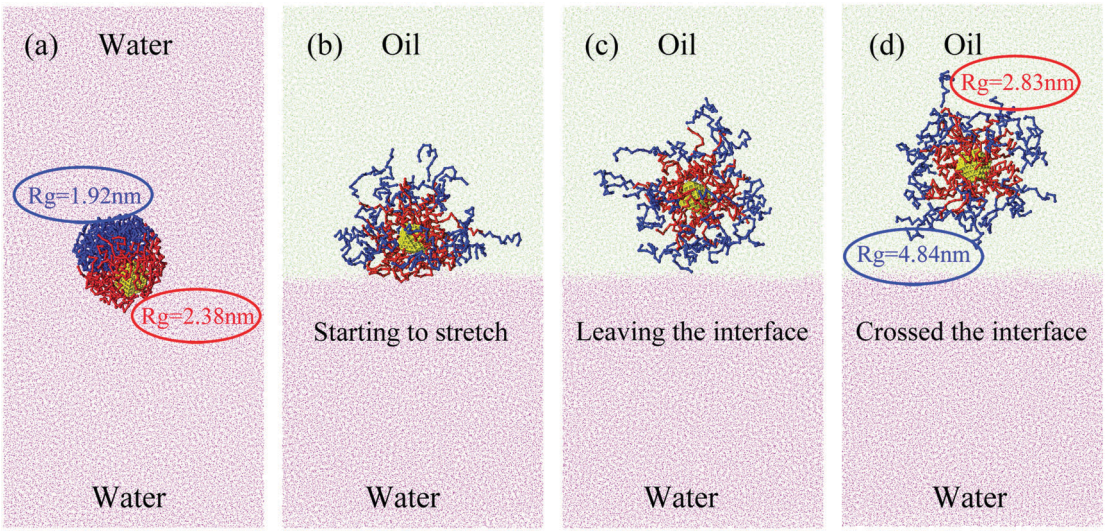

Fig. 4 Phase transfer process of AuNP modified functionalized weak hydrophilic/hydrophobic BA diblock polymer brushes (hydrophobic chains as outer blocks while weak hydrophilic chains as inner blocks. Yellow: Au beads; blue: hydrophobic beads; red: hydrophilic beads).

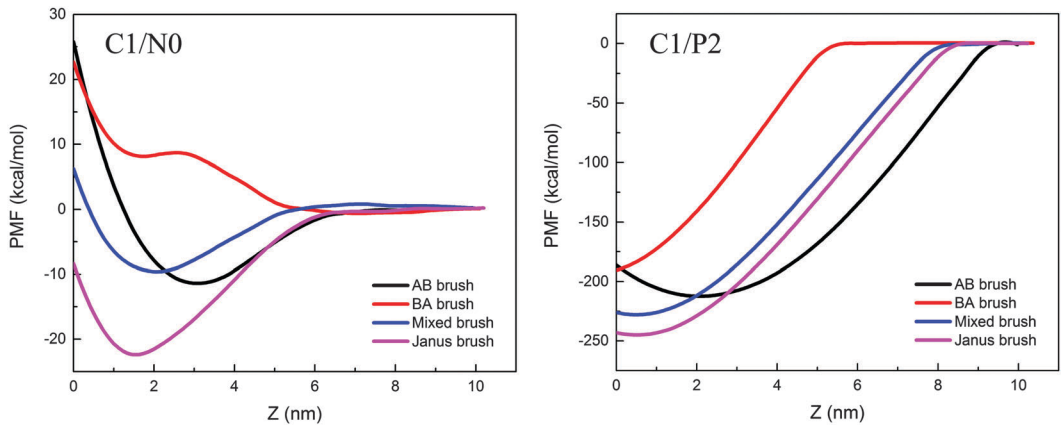

Fig. 5 Potential of mean force along the *Z* direction for each of the functionalized NPs: removing from the oil–water interface into the oil phase. Left panel: AuNPs grafted with hydrophobic/weak hydrophilic brushes (C1/N0 systems); right panel: AuNPs grafted with hydrophobic/strong hydrophilic brushes (C1/P2 systems).

was also been confirmed by atomistic MD simulations (Fig. S3, ESI†). This phenomenon is consistent with the experimental and simulation studies.[18,22,51]

Hydrophobic/strong hydrophilic polymer brush-grafted AuNPs (C1/P2 systems). It has been confirmed that the properties of polymer-brush-functionalized NPs can be tuned by changing the chemical nature of brushes.[8] In this work, we increased the hydrophilicity from N0 to P2 (similar to PVA), and these model systems correspond to the AuNPs modified with hydrophobic chains and quite strong hydrophilic chains. As shown in Fig. 3, the morphologies of functionalized AuNPs are quite different from those of C1/N0 systems.

We focused on the conformations formed in the pure water phase at first. For AB brush-grafted AuNPs, a core–shell structure is formed with a hydrophobic C1 core and a hydrophilic P2 shell. The hydrophilic shell is stretched out in the water phase due to the stronger hydrophilicity of the P2 blocks. It can be found that the BA brush-functionalized AuNP shows a worm-like morphology, and the mixed brush and Janus brush-grafted NPs present a jellyfish-like conformation, which has been demonstrated in our previous work.[50] In the oil–water bi-phase system, all functionalized AuNPs are trapped in the interface region instead of transferring into any phase, with the gold core remaining at the interface, while hydrophilic and hydrophobic chains being in their respective good solvent. In this case, the interaction between hydrophilic chains and water is almost the same as that between hydrophobic chains and oil; both hydrophobic and hydrophilic chains can hardly extend to their good solvent due to the mutual hauling effect. As for the morphologies, a ''hat'' structure is formed for the AB brush-modified NPs, while the rest systems present a ''Janus'' conformation. Further observation shows that the degree of phase separation of the ''Janus'' structure within the three systems (BA diblock brush, mixed brush and Janus brush-modified NPs)

gradually increases. For Janus brush-functionalized NPs, there is no contact between the hydrophilic and hydrophobic chains. All morphologies can be demonstrated by the brush density profiles.

Therefore, it indicates that the grafting architecture of polymer brushes could have a significant effect on the interfacial behaviours of functionalized NPs at the oil–water interface. It is worth expecting that, with proper regulation of the composition and architecture of the grafted polymer brushes, these systems could have good performance in various applications such as biomaterials, controlled drug delivery vehicles, and Pickering emulsion catalysis.

3.2 Equilibrium positions of functionalized AuNPs

The distribution of the centre of AuNPs is calculated by density profiles along the z axis to decide whether the functionalized AuNPs can pass through the interface completely. In this work, we chose the oil–water interface as the zero position in the z direction, which can be distinguished by analyzing the water and oil density profiles. Negative values represent that functionalized AuNPs remain in the water phase while the positive values mean that functionalized AuNPs remain in the oil phase. In order to show results as clear as possible, the interface region was defined within the range of z coordinates from -2 to 2 nm.[51] Considering the size of AuNPs themselves, the equilibrium position of NPs that can break the interface region and completely transfer from the water to oil phase should be larger than 6 nm, the positions where most AuNP centres focused on are treated as the equilibrium positions in the following discussions. All equilibrium positions of AuNP centres of the studied systems are summarized in Table 1.

As is shown in Table 1, it is interesting to notice that the situation, when the equilibrium position of the AuNP centre exceeds 6 nm, only occurs for BA polymer-brush-modified AuNPs (hydrophobic chains as outer blocks while weak hydrophilic chains as inner blocks) in the C1/N0 systems, demonstrating their ability of phase transfer. Besides, the functionalized AuNPs in C1/P2 systems tend to remain in the oil–water interface region when compared with those in C1/N0 systems. This reflects a stronger interfacial activity and stability to some extent, mainly because of the increased hydrophilicity of these functionalized AuNPs.

3.3 Phase transfer behaviour and mechanism

From the above analysis, we conclude that the AuNP functionalized with hydrophobic (C1) and weak hydrophilic (N0) chains can break up the interface region and draw the particle into the oil phase. In order to investigate the mechanism of phase transfer behaviour, we choose the BA diblock polymer brush-grafted AuNP (hydrophobic chains as outer blocks while weak hydrophilic chains as inner blocks) as an example, for which the particle can wholly move into the oil phase.

As shown in Fig. 4, the whole processes of phase transfer can be divided into four stages: (1) first, the functionalized AuNP achieved equilibrium in the water phase, and all brushes are bent on the surface of the gold core. A "Janus" conformation is formed due to the exposure of inner hydrophilic N0 blocks (Fig. 4a). (2) Second, when some of the outer hydrophobic blocks come into contact with the oil phase, they soon extend and become coiled. These activated brushes can fluctuate and activate other brushes around them, and thus enhance the mobility of linked blocks. As we can see from Fig. 4b, almost all brushes extend even though the oil phase is the poor solvent for hydrophilic blocks (N0). The enhanced flexibility of the brushes offers the NP more mobility and further make more brushes contact with the oil phase (Fig. 4b). (3) Third, as the interaction between hydrophobic blocks and the oil phase dominates, the functionalized AuNP gradually moves into the oil phase with more brushes stretched out (Fig. 4c). (4) Lastly, the whole particle moves into the oil phase completely with no brushes contacting with the interface (Fig. 4d). This is also consistent with the results of all-atom MD simulations (see Fig. S4, ESI†).

To find the underlying mechanism of phase transfer behaviour, the radius of gyration (R_g) of each block is computed and marked in the graph before and after the functionalized AuNP crosses the interface region. As shown in Fig. 4a, after the NP moves into the oil phase completely, R_g values of both hydrophilic blocks and hydrophobic blocks increase. R_g of the hydrophilic blocks changes from 2.38 nm to 2.83 nm, while that of the hydrophobic blocks increases from 1.92 nm to 4.84 nm, presenting a bigger alteration. The extension of the hydrophobic blocks in the oil phase can fluctuate and affect the linked hydrophilic blocks.

The traction effect between the linked blocks as well as the unfavourable interactions between the hydrophilic blocks and the oil phase make the R_g of the hydrophilic blocks change a little. This means that the flexibility of outer blocks has a significant effect on the phase transfer process. Besides, as demonstrated before, other three systems are trapped in the interface region and only partial phase transfer occurs. All these indicate that the grafting architecture of polymer brushes plays a significant role in the interfacial behaviours of functionalized AuNPs at the oil–water interface; the block sequence of brushes is also a dominant factor to decide whether a AuNP can accomplish phase transfer completely, or be restricted in the interface region.

3.4 Desorption energy of functionalized AuNPs

In most cases, the amphiphilic NPs tend to remain in the oil–water interface region. The energy required to move NPs from the interface region into one of the homogeneous phases, namely desorption energy, is a very important indicator which reflects the interfacial activities and stability of NPs at the interface. In this work, for most studied systems (such as C1/N0 systems), the functionalized AuNPs can cross the interface and move into the oil phase partially or completely. To save computational resources, we simply computed the desorption energy of the functionalized AuNPs from the interface region to the oil phase, and it is sufficient to reflect the interfacial activities and stability of NPs in the interface region. The functionalized AuNPs were placed at the oil–water interface and moved into the oil phase completely by exerting a pulling force along the z direction. The PMF curves are plotted as a

function of the distance from the interface in Fig. 5. PMF describes the free energy required for the deviation of NPs from their equilibrium position along the normal to the interface region, and the desorption energy was then estimated by the free energy changes after the NPs were pulled from the interface region into the oil phase completely.[25]

As shown in Fig. 5, for C1/N0 systems, almost all of the PMFs decrease rapidly first and then grow with the increase of the distance between the center of mass of NPs and the interface region. The minimum corresponds to the stable state of NPs, as demonstrated in Section 3.1. After the NP was pulled into the oil phase, the PMF flattened. Thus, the NPs must overcome the energy barrier to depart from the oil–water interface. However, for BA polymer-brush-grafted AuNPs (hydrophobic chains as outer blocks while weak hydrophilic chains as inner blocks) in C1/N0 systems, the PMF keeps decreasing with the increase of the distance until the NP moves into the oil phase, this is due to the fact that the functionalized AuNP can completely cross the interface region spontaneously. For C1/P2 systems, the PMFs increase with the increase of the distance except for AB brush-modified AuNPs, and the position of the minimum value is closer to the interface region due to the enhanced hydrophilicity.

To clearly discuss the interfacial activities and stability of functionalized AuNPs in a quantitative manner, we summarize the values of the desorption energy of all systems and list them in Table 2. For functionalized AuNPs in C1/N0 systems, the grafting architecture of polymer brushes can significantly influence the desorption energy for NPs to leave the interface region. The values of AB brushes (hydrophobic chains as inner blocks while weak hydrophilic chains as outer blocks) and mixed brush-functionalized AuNPs are almost equal, while the desorption energy of Janus brush-modified AuNP is more than 2 times of the mixed one. This is consistent with Binks and co-workers' theoretical work which confirmed that the Janus NPs have desorption energy about three times higher than the corresponding homogeneous NPs.[58] Robert also demonstrated that suitable Janus particles can have a maximum desorption free energy with 3 times the maximum magnitude of that for homogeneous particles of the same size.[59] These further prove the reasonability of our CG models and methods. However, as the hydrophilicity of hydrophilic chains is tuned from N0 to P2, the desorption energy of grafted AuNPs in C1/P2 systems is considerably increased, when compared with those in the C1/N0 systems. In both cases, the Janus brush-grafted AuNPs show the highest desorption energy, indicating a higher interfacial activity.

We conclude that interfacial behaviours of functionalized AuNPs can be modulated by tuning the grafting architecture and the chemical nature of polymer brushes. It has been demonstrated that the amphiphilic Janus particles can exhibit an interfacial activity several times higher than simple homogeneous particles.[58] Janus particles combine the amphiphilic character of surfactants and the physical properties of NPs, which opens new opportunities in emerging areas of nanotechnology and emulsion stabilization.[60] Thus this work could provide some guidance for the design and production of emulsion stabilizers with better performance.

4. Conclusions

In this work, we performed coarse-grained simulations based on the MARTINI force field to investigate the interfacial behaviors of polymer brush-functionalized NPs with various grafting architectures (diblock brush, mixed brush and Janus brush grafted gold NPs) at the oil–water interface. Simulation results show that functionalized NPs present abundant morphologies including typical core–shell, Janus-type, jellyfish-like, hamburger-like and others, depending on the solvent environment, the hydrophobicity and grafting architecture of polymer brushes. It is found that AuNPs grafted with hydrophobic/weak hydrophilic polymer brushes (C1/N0 systems) have better phase transfer performance, especially for weak hydrophilic–hydrophobic diblock polymer-brush-grafted AuNPs, which can cross the interface region and move into the oil phase completely. However, for AuNPs modified with hydrophobic/strong hydrophilic polymer brushes (C1/P2 systems), all AuNPs are trapped in the interface region instead of transferring into any phase, with the gold core remaining at the interface, while hydrophilic and hydrophobic chains being in their respective good solvent. The mechanism of phase transfer behaviour has been explained, and the whole phase transfer process can be divided into four stages: (1) first, the modified NP achieved equilibrium in the water phase; all brushes are bent on the surface of the gold core. (2) Second, when some of the outer hydrophobic blocks come into contact with the oil phase they would soon extend and become coiled. These activated brushes can fluctuate and activate other brushes around them, and thus enhance the flexibility of linked blocks. (3) Third, as the interaction between hydrophobic blocks and oil phase dominates, the NP gradually moves into the oil phase and more brushes stretch out. (4) Lastly, the whole particle moves into the oil phase completely. It is believed that the flexibility of outer blocks plays an important role in the phase transfer process. The functionalized NPs with excellent phase transfer ability have potential in many applications, particularly in phase transfer catalysis and drug delivery. In addition, the desorption energy of each functionalized AuNPs moving from the interface region into the oil phase was obtained from PMF analysis. The results demonstrate that Janus brush-grafted AuNPs show the highest interfacial activity and stability, and this can be further strengthened by increasing the hydrophilicity of grafted polymer brushes. This implies that the Janus brush-grafted AuNPs exhibit better performance when used as emulsifiers to stabilize the emulsion.

It was expected that this work could provide some useful information and guidance on the development and applications of this new kind of polymer–NP composite nanomaterial.

Acknowledgements

Support from the National Key Basic Research Program of China (No. 2013CB733500), National Natural Science Foundation of China (No. 21376089 and 91334202), Guangdong Science Foundation (No. S2011010002078 and 2014A030312007) and the Fundamental Research Funds for the Central Universities (SCUT-2015ZP033) is gratefully acknowledged. An allocation

time from the SCUTGrid at South China University of Technology is also gratefully acknowledged.

Notes and references

1 B. Zhao and L. Zhu, *Macromolecules*, 2009, **42**, 9369–9383.
2 Y. Chen, *Macromolecules*, 2012, **45**, 2619–2631.
3 M. G. Moffitt, *J. Phys. Chem. Lett.*, 2013, **4**, 3654–3666.
4 J. Shan and H. Tenhu, *Chem. Commun.*, 2007, 4580–4598.
5 C. Y. Li, B. Zhao and L. Zhu, *J. Polym. Sci., Part B: Polym. Phys.*, 2014, **52**, 1581–1582.
6 Y. Liu, Y. Liu, J.-J. Yin and Z. Nie, *Macromol. Rapid Commun.*, 2015, **36**, 711–725.
7 L. Chen and H.-A. Klok, *Soft Matter*, 2013, **9**, 10678–10688.
8 X. C. Luu and A. Striolo, *J. Phys. Chem. B*, 2014, **118**, 13737–13743.
9 J. Wang and M. Muller, *J. Phys. Chem. B*, 2009, **113**, 11384–11402.
10 S. Tsuji and H. Kawaguchi, *Macromolecules*, 2006, **39**, 4338–4344.
11 D. Pissuwan, T. Niidome and M. B. Cortie, *J. Controlled Release*, 2011, **149**, 65–71.
12 C. E. Estridge and A. Jayaraman, *ACS Macro Lett.*, 2015, **4**, 155–159.
13 C. Bao, J. M. Horton, Z. Bai, D. Li, T. P. Lodge and B. Zhao, *J. Polym. Sci., Part B: Polym. Phys.*, 2014, **52**, 1600–1619.
14 J. W. O. Salari, F. A. M. Leermakers and B. Klumperman, *Langmuir*, 2011, **27**, 6574–6583.
15 B. P. Binks and S. O. Lumsdon, *Langmuir*, 2000, **16**, 8622–8631.
16 M. Angel Fernandez-Rodriguez, Y. Song, M. Angel Rodriguez-Valverde, S. Chen, M. Angel Cabrerizo-Vilchez and R. Hidalgo-Alvarez, *Langmuir*, 2014, **30**, 1799–1804.
17 Y. Wang, D. Fan, J. He and Y. Yang, *Colloid Polym. Sci.*, 2011, **289**, 1885–1894.
18 L. Song, H. Sun, X. Chen, X. Han and H. Liu, *Soft Matter*, 2015, **11**, 4830–4839.
19 J. M. Horton, Z. Bai, X. Jiang, D. Li, T. P. Lodge and B. Zhao, *Langmuir*, 2011, **27**, 2019–2027.
20 D. Li and B. Zhao, *Langmuir*, 2007, **23**, 2208–2217.
21 Y. Wu, C. Zhang, X. Qu, Z. Liu and Z. Yang, *Langmuir*, 2010, **26**, 9442–9448.
22 S. Sekiguchi, K. Niikura, Y. Matsuo and K. Ijiro, *Langmuir*, 2012, **28**, 5503–5507.
23 L. Cheng, A. Liu, S. Peng and H. Duan, *ACS Nano*, 2010, **4**, 6098–6104.
24 D. Li, C. Li, Y. Yang, Q. He and J. Li, *J. Nanosci. Nanotechnol.*, 2011, **11**, 2052–2056.
25 H. Fan, D. E. Resasco and A. Striolo, *Langmuir*, 2011, **27**, 5264–5274.
26 X. C. Luu, J. Yu and A. Striolo, *Langmuir*, 2013, **29**, 7221–7228.
27 D. L. Cheung and P. Carbone, *Soft Matter*, 2013, **9**, 6841–6850.
28 H. Gao, Z. Lu, H. Liu, Z. Sun and L. An, *J. Chem. Phys.*, 2014, **141**, 134907.
29 K. Schwenke, L. Isa, D. L. Cheung and E. Del Gado, *Langmuir*, 2014, **30**, 12578–12586.
30 P. Espanol and P. Warren, *Europhys. Lett.*, 1995, **30**, 191–196.
31 P. J. Hoogerbrugge and J. M. V. A. Koelman, *Europhys. Lett.*, 1992, **19**, 155–160.
32 R. D. Groot and P. B. Warren, *J. Chem. Phys.*, 1997, **107**, 4423–4435.
33 J. Cheng, A. Vishnyakov and A. V. Neimark, *Langmuir*, 2014, **30**, 12932–12940.
34 H. Liu, H. Guo and J. Zhou, *Acta Chim. Sin.*, 2012, **70**, 2445–2450.
35 H. Y. Guo, X. Q. Qiu and J. Zhou, *J. Chem. Phys.*, 2013, **139**, 084907.
36 X. Guo, L. Zhang, Y. Qian and J. Zhou, *Chem. Eng. J.*, 2007, **131**, 195–201.
37 J. He, X. Huang, Y.-C. Li, Y. Liu, T. Babu, M. A. Aronova, S. Wang, Z. Lu, X. Chen and Z. Nie, *J. Am. Chem. Soc.*, 2013, **135**, 7974–7984.
38 Y. Liu, Y. Li, J. He, K. J. Duelge, Z. Lu and Z. Nie, *J. Am. Chem. Soc.*, 2014, **136**, 2602–2610.
39 S. J. Marrink, A. H. de Vries and A. E. Mark, *J. Phys. Chem. B*, 2004, **108**, 750–760.
40 S. J. Marrink, H. J. Risselada, S. Yefimov, D. P. Tieleman and A. H. de Vries, *J. Phys. Chem. B*, 2007, **111**, 7812–7824.
41 G. Yu, J. Liu and J. Zhou, *J. Phys. Chem. B*, 2014, **118**, 4451–4460.
42 M. Bulacu, N. Goga, W. Zhao, G. Rossi, L. Monticelli, X. Periole, D. P. Tieleman and S. J. Marrink, *J. Chem. Theory Comput.*, 2013, **9**, 3282–3292.
43 G. Yu, J. Liu and J. Zhou, *AIChE J.*, 2015, **61**, 2035–2047.
44 G. Rossi, L. Monticelli, S. R. Puisto, I. Vattulainen and T. Ala-Nissila, *Soft Matter*, 2011, **7**, 698–708.
45 H. Lee, A. H. de Vries, S.-J. Marrink and R. W. Pastor, *J. Phys. Chem. B*, 2009, **113**, 13186–13194.
46 H. Chan and P. Kral, *Nanoscale*, 2011, **3**, 1881–1886.
47 S. J. Marrink and D. P. Tieleman, *Chem. Soc. Rev.*, 2013, **42**, 6801–6822.
48 J. Lin, H. Zhang, Z. Chen, Y. Zheng, Z. Zhang and H. Ye, *J. Phys. Chem. C*, 2011, **115**, 18991–18998.
49 J. Lin, H. Zhang, Z. Chen and Y. Zheng, *ACS Nano*, 2010, **4**, 5421–5429.
50 J. Dong and J. Zhou, *Macromol. Theory Simul.*, 2013, **22**, 174–186.
51 J. Dong, J. Li and J. Zhou, *Langmuir*, 2014, **30**, 5599–5608.
52 J. Koski, H. Chao and R. A. Riggleman, *Chem. Commun.*, 2015, **51**, 5440–5443.
53 A. S. Almusallam and D. S. Sholl, *J. Colloid Interface Sci.*, 2007, **313**, 345–352.
54 Y. Shi, V. Selin, Y. Wang and S. A. Sukhishvili, *Part. Part. Syst. Charact.*, 2013, **30**, 950–957.
55 T. Zhou, B. Dong, H. Qi, S. Mei and C. Y. Li, *J. Polym. Sci., Part B: Polym. Phys.*, 2014, **52**, 1620–1640.
56 B. Hess, C. Kutzner, D. van der Spoel and E. Lindahl, *J. Chem. Theory Comput.*, 2008, **4**, 435–447.
57 W. Humphrey, A. Dalke and K. Schulten, *J. Mol. Graphics*, 1996, **14**(3338), 27–38.
58 B. P. Binks and P. D. I. Fletcher, *Langmuir*, 2001, **17**, 4708–4710.
59 R. Aveyard, *Soft Matter*, 2012, **8**, 5233–5240.
60 A. Boeker, J. He, T. Emrick and T. P. Russell, *Soft Matter*, 2007, **3**, 1231–1248.